Contribution from the Department of Chemistry, University of New Orleans, Lakefront, New Orleans, Louisiana 70122, and the Chemistry Division, Savannah River Laboratory, E. I. du Pont de Nemours and Company, Aiken, South Carolina 29808

Metal Ion Complexes of α-Amido Acids. 2. Structure and Magnetic Properties of Iron(II) Hippurate, a Linear-Chain Insulator

MAURICE M. MORELOCK,[1a] MARY L. GOOD,*[1b] LOUIS M. TREFONAS,*[1a] RICHARD MAJESTE,[1c] and DAVID G. KARRAKER*[1d]

Received February 19, 1982

Iron(II) hippurate, $Fe(hipp)_2(H_2O)_3 \cdot 2H_2O$, has been prepared and characterized. Single-crystal X-ray diffraction revealed the compound to be essentially isostructural with the previously reported cobalt(II) and nickel(II) hippurates, crystallizing as a linear chain with canted metal octahedra bridged by the oxygen atom of a water molecule. The space group is $C2/c$ with four formula weights per unit cell. The structural properties for the compound are $a = 40.824$ (7) Å, $b = 6.908$ (1) Å, $c = 8.038$ (1) Å, and $\beta = 91.6$ (1)°; the intrachain Fe–Fe′ distance is 4.017 Å, with $R = 0.136$ for 529 reflections. A magnetic model assuming a one-dimensional Ising chain with a magnetic phase transition at 8.1 K is consistent with the observed powder magnetic susceptibility and temperature-dependent Mössbauer data.

Introduction

An earlier communication[2] and a full paper[3] from our laboratory reported the structure and magnetic properties for the essentially isostructural cobalt(II) and nickel(II) hippurates (hippurate is $C_6H_5CONHCH_2CO_2^-$). The site symmetry of the metal ions was essentially C_{2h} with two hippurate ions (bonded through a single carboxyl oxygen) and two water molecules in the central plane and two bridging (through the oxygen atom) water molecules in the axial positions. The unit cell indicated that the linear chains were arranged in "rows" with interchain hydrogen bonding. The intrachain metal–metal distance was about 4 Å, and the interchain distances were appoximately 7 Å within the "rows" and 20 Å between "rows". The magnetic susceptibility data taken for powder samples as a function of temperature and field strength indicated a metamagnetic transition at low temperatures for the Co(II) complex and exhibited a broad maximum in the $1/\chi$ vs. T curve for the Ni(II) complex. A consideration of the structure and the observed magnetic properties led us to propose a qualitative model where cooperative magnetic phenomena produced a low-dimensional magnetic effect. The *possible* magnetic-exchange phenomena were assumed to be (1) isotropic, antiferromagnetic superexchange along the chain (c axis), (2) anisotropic [Dzyaloshinsky–Moriya (D–M)[4,5]], antiferromagnetic superexchange along the chain, and (3) dipole–dipole interactions between chains (b axis). As the temperature was lowered, the model was consistent with a sequence of events where antiferromagnetic superexchange via the bridging water molecules was followed by the production of a net spontaneous moment along the chain generated by the canted spins through the D–M interaction. The magnitude of the single-ion anisotropy of the Co(II) ion was expected to be significantly greater than that exhibited by the Ni(II) system, thus producing a larger net moment along the chain. This prediction was borne out by the observation of the very low temperature, metamagnetic transition in the Co(II) system, which we attributed to the dipole–dipole interaction between neighboring chains in the "rows" resulting in an antiferromagnetic coupling of adjacent chains. Thus this series of α-amido acid complexes provides a new set of materials for investigating the relationship between detailed structural parameters and magnetic properties and may provide experimental data for evaluating magnetic models for low-dimensional systems. This paper reports the extension of the work to the corresponding Fe(II) system, where the structural and magnetic data can be augmented by temperature-dependent Mössbauer spectra.

Experimental Section

Synthetic Procedures. Since iron(II) hippurate proved to be an air-sensitive material, Schlenk-type glassware was used for its preparation. The solvent (50:50 water–ethanol) was degassed for 20–30 min; during this time the Schlenk apparatus was evacuated and filled with argon gas. A 30-mL quantity of the solvent was then added to an addition flask under positive argon pressure; 0.01 mol of $Fe(ClO_4)_2 \cdot 6H_2O$ and about 0.5 g of Fe filings (100 mesh) were also added to this flask and stirred via a magnetic bar.[6] While trace amounts of Fe(III) were reducing, 0.02 mol of sodium hippurate and 75 mL of degassed solvent were added to the reaction flask. When the iron perchlorate solution exhibited only the pale blue-green color characteristic of aqueous Fe(II), the metal ion solution was added to the reaction flask containing the hippurate ligand. Crystallization began within 5 min and was usually complete in about 1 h. The solvent was then aspirated out of the reaction flask and replaced with fresh, degassed solvent. The crystals were dissolved by gentle heating; the iron fillings were then filtered off by a medium-porosity sintered-glass disk, and recrystallization was allowed to proceed in the filtrate flask. Once recrystallization was complete, the compound was filtered off by a second sintered-glass disk; the crystals were dried by flowing argon over them for approximately 1 h. The crystals were then collected into several individual sample vials by utilizing a "cow" receptacle. A slight vacuum was created within the apparatus so that the sample vials could be cut off with a gas torch. This technique provided individual samples for elemental analysis and subsequent physical characterization experiments. Sample vials were left sealed until used. The vials were opened in a drybox, and all subsequent sample preparation was carried out in the drybox. Air oxidation, when it occurred, was easily recognized by the yellow ferric coloration that formed on the exposed crystal edges and faces.

All samples were polycrystalline powders (except those grown for X-ray analysis). Elemental analysis, including careful determination of total water by thermal gravimetric techniques, provided the overall stoichiometry of the complexes. Representative results for $Fe(C_6H_5CONHCH_2CO_2)_2(H_2O)_3 \cdot 2H_2O$ were as follows. Anal. Calcd: C, 43.04; H, 5.18; N, 5,58; Fe, 11.13; H_2O, 17.9. Found: C, 43.08; H, 5.39; N, 5.48; Fe, 11.97; H_2O, 18.3.

Collection, Reduction, and Refinement of X-ray Crystallographic Data. Single crystals of the iron hippurate grow in very thin rectangular plates. Consequently, growing a crystal even minimally suitable for an X-ray diffraction study proved to be difficult. The

(1) (a) University of New Orleans. (b) Corporate Research Center, UOP, Inc., Des Plaines, IL 60016. (c) Chemistry Department, Southern University in New Orleans. (d) E. I. du Pont de Nemours and Co.
(2) H. Eichelberger, R. Majeste, R. Surgi, L. Trefonas, M. L. Good, and D. Karraker, *J. Am. Chem. Soc.*, **99**, 616 (1977).
(3) M. M. Morelock, M. L. Good, L. M. Trefonas, L. Maleki, H. R. Eichelberger, R. Majeste, J. Dodge, and D. Karraker, *J. Am. Chem. Soc.*, **101**, 4858 (1979).
(4) I. Dzyaloshinsky, *J. Phys. Chem. Solids*, **4**, 241 (1958).
(5) (a) T. Moriya, *Phys. Rev.*, **120**, 91 (1960); (b) T. Moriya, *Magnetism*, **1**, Chapter 3 (1963).
(6) It should be pointed out that other reducing agents were tried but were not successful. For example, sodium dithionite interferes with the synthesis and precipitates the iron as a dark green solid. A zinc–mercury amalgam cannot be used since the zinc hippurate is not isomorphous with the iron, nickel, and cobalt series. The only reducing agent we found satisfactory was pure iron metal, where the reduction reaction resulted in only aqueous Fe(II).

0020-1669/82/1321-3044$01.25/0 © 1982 American Chemical Society

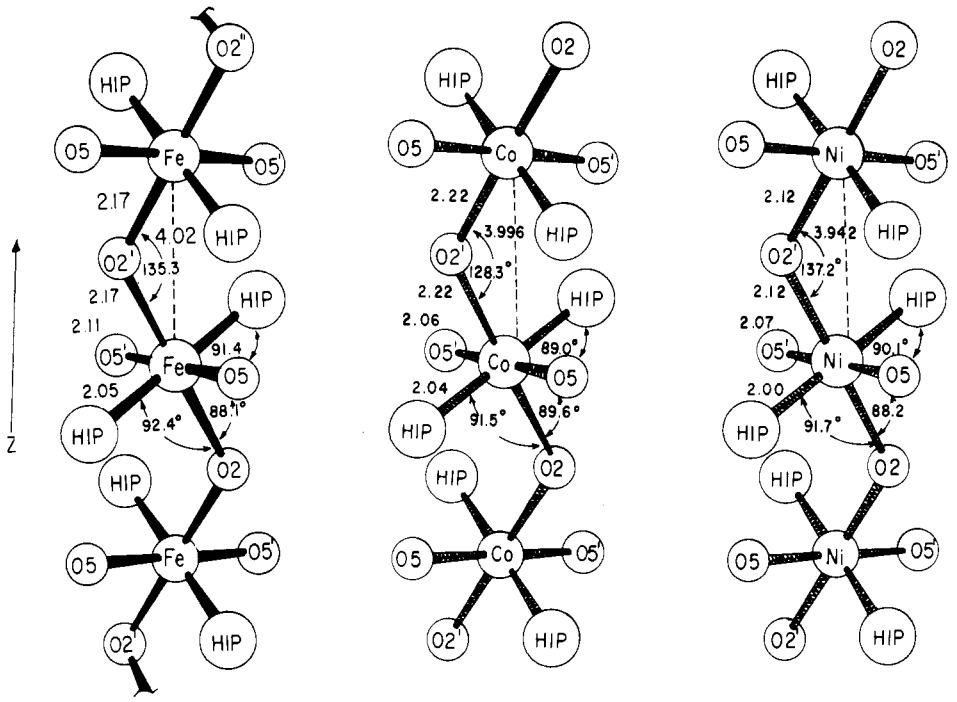

Figure 1. Projection view of the site symmetry about the Fe(II), Co(II), and Ni(II) ions.

crystal finally chosen (no dimension in the face of the plate greater than 0.2 mm and a thickness of 0.05 mm) was mounted in a glass capillary. This was necessary because the crystals oxidize and collapse on extended exposure to the air. Preliminary symmetry studies with a General Electric XRD-5 diffractometer and Cu Kα radiation showed the iron hippurate to be essentially isomorphous with the previously determined nickel and cobalt hippurates;[3] systematic extinctions (hkl, $h + k = 2n + 1$; $h0l$, $l = 2n$) were observed and confirmed the previous space-group choice of $C2/c$. Lattice constants were determined by a least-squares fit of 18 carefully measured values of the copper $K\alpha_1$ and $K\alpha_2$ doublet for reflections with $2\theta > 70°$ under fine conditions (1° takeoff angle and 0.05° slit). The resultant lattice constants and their estimated standard deviations (esd) are as follows (the nickel and cobalt hippurate results are reproduced for comparative purposes):

	Fe	Ni	Co
a, Å	40.824 (7)	40.833	40.823
b, Å	6.908 (1)	6.928	6.903
c, Å	8.038 (1)	7.884	7.992
β, deg	91.6 (1)	91.9	91.9

The calculated density of 1.38 g/cm³ for four molecules per unit cell is in agreement with experimentally measured densities for these metal hippurates. Three-dimensional intensity data were collected with use of balanced nickel and cobalt filters. A total of 1403 independent reflections were measured to a 2θ maximum of 100°. Of these, 529 (37%) were considered statistically significant by the criterion

$$[I_{Ni} - 2\sigma(I_{Ni})] - [I_{Co} - 2\sigma(I_{Co})] > T$$

where T is a function of the background cutoff. T was chosen to be 75 for this compound while the σ values were determined by counting statistics. The usual intensity corrections ($1/Lp$, α_1–α_2 splitting, decay) were applied, and a rough cylindrical approximation was made for the absorption as a function of φ.

Refinement of the iron hippurate structure was begun with atom positions that were approximated by adjusting the refined atom parameters obtained in the isomorphous cobalt and nickel structures. Local problems led to the data being taken with copper radiation although it was recognized that this would lead to absorption edge difficulties. Attempts to rectify this problem, and the added problem of poor crystal quality, through an appropriate absorption correction were only partially successful. Hence the structure has been refined[7] only to a value of $R = 0.136$.

Magnetic Susceptibility Data. Low-temperature magnetic data (2.2–80 K) were determined with a Foner-type vibrating-sample magnetometer (manufactured by Princeton Applied Research Corp.) operated in the field of a 12-in. electromagnet. A germanium resistance thermometer mounted directly behind the sample measured the temperatures, which were corrected for magnetic field. At 8 K the correction was 0.15. All systems were calibrated with a piece of pure Ni metal.

Mössbauer Spectral Data. Initial Mössbauer data were obtained at room temperature, 77 K, and 4.2 K on an Austin Science Associates Mössbauer spectrometer with laser velocity calibration and a Janis Model 8DT Super Vari-temp stainless steel Dewar. ^{57}Co diffused into a copper matrix was the source of the 14.4 keV ^{57}Fe γ rays. Data reduction was accomplished with a conventional least-squares Lorentzian line shape program[8] on a PDP-10 computer. Subsequent detailed spectra as a function of temperature below 20 K were obtained in Dr. William Reiff's laboratory at Northeastern University. The Mössbauer spectrometer was similar to the one described above in use in our laboratory. Temperature control was achieved with an uncalibrated silicon diode coupled to a Lake Shore Cryotronics Model DT-500C set point controller. Temperature measurements were made with a Leeds and Northrup K-4 potentiometer on a six-phase Dana Model 5330 digital voltmeter with a calibrated silicon diode driven by a 10-A constant-current source. The temperature stability was continuously monitored by following the error signal of a silicon diode (50 mV/K) after precise compensation via the K-4 potentiometer and was typically of the order of ±0.005 K.

Sub-helium temperatures were obtained through controlled pumping (LJ Engineering Model 329 vacuum regulator valve) on the Janis cryostat diffuser assembly. The temperature was determined from the vapor pressure of helium measured by a Wallace-Tiernon Model FA-160 absolute-pressure gauge.

Least-squares Lorentzian fits to the resulting Mössbauer spectra were accomplished with the computer program developed by Stone.[9]

Results

Crystallographic Structure. The final least-squares coordinates and temperature factors (with estimated standard deviations) for each parameter are summarized in Table I. Esd values of 0.02 Å for Fe–O distances and 0.7° for O–Fe–O angles are double the values for the cobalt hippurate and

(7) The conventional reliability index $R = \sum w||kF_o| - |kF_c||/\sum w|kF_o|$ is cited throughout the paper. Scattering factors for carbon, nitrogen, oxygen, and iron are taken from the paper by D. T. Cramer and J. T. Waber, *Acta Crystallogr.*, **18**, 104 (1965).

(8) S. W. Marshall, J. A. Nelson, and R. M. Wilenzick, *Commun. ACM*, **8**, 313 (1965).

(9) G. M. Bancroft, A. G. Maddock, W. K. Ong, R. H. Prince, and A. J. Stone, *J. Chem. Soc. A*, 1966 (1967).

Table I. Fractional Coordinates and Anisotropic Thermal Parameters[a] (Standard Deviations ×10⁴ in Parentheses)

atom	x	y	z	β_{11}	β_{22}	β_{33}	β_{12}	β_{13}	β_{23}
Fe	0.5000 (0)	0.5000 (0)	0.5000 (0)	3 (0)	108 (16)	162 (15)	0 (4)	1 (2)	22 (18)
O1	0.4647 (5)	0.3101 (32)	0.5735 (26)	5 (2)	155 (59)	110 (46)	0 (9)	1 (7)	−24 (46)
O2	0.5000 (0)	0.6197 (62)	0.7500 (0)	0 (2)	443 (-)	373 (-)	0 (0)	10 (12)	0 (0)
O3	0.4424 (6)	0.2301 (34)	0.3238 (29)	6 (2)	205 (67)	163 (52)	−2 (10)	−3 (8)	−64 (50)
O4	0.3673 (7)	0.3667 (39)	0.4176 (40)	10 (3)	196 (80)	411 (86)	−8 (13)	−6 (13)	60 (69)
O5	0.4642 (5)	0.6999 (30)	0.4149 (26)	6 (2)	103 (53)	109 (46)	−10 (9)	−1 (7)	28 (44)
O6	0.4009 (6)	0.3210 (34)	0.0376 (33)	4 (2)	157 (63)	315 (69)	1 (10)	4 (9)	−16 (59)
N1	0.3862 (6)	0.0864 (41)	0.4709 (37)	0 (2)	177 (74)	244 (72)	−6 (10)	−6 (9)	45 (61)
C1	0.4414 (9)	0.2366 (40)	0.4841 (42)	8 (3)	−15 (73)	141 (71)	−1 (14)	22 (12)	27 (61)
C2	0.4135 (7)	0.1572 (45)	0.5794 (45)	1 (2)	90 (87)	235 (85)	5 (11)	7 (11)	89 (74)
C3	0.3648 (7)	0.1923 (45)	0.4041 (56)	1 (2)	6 (71)	502 (-)	3 (11)	−21 (14)	28 (87)
C4	0.3357 (10)	0.1184 (52)	0.3187 (51)	8 (3)	104 (96)	263 (-)	0 (16)	16 (16)	39 (83)
C5	0.3127 (9)	0.2303 (61)	0.2341 (49)	5 (3)	304 (-)	204 (91)	18 (17)	−15 (13)	15 (90)
C6	0.2841 (10)	0.1643 (68)	0.1519 (54)	6 (3)	426 (-)	261 (-)	31 (21)	−28 (16)	−83 (-)
C7	0.2805 (10)	−0.0360 (64)	0.1466 (57)	6 (3)	284 (-)	369 (-)	−4 (19)	7 (16)	−152 (-)
C8	0.3024 (9)	−0.1428 (61)	0.2003 (59)	3 (3)	264 (-)	408 (-)	−5 (18)	−15 (16)	−23 (-)
C9	0.3303 (9)	−0.0850 (60)	0.2883 (52)	6 (3)	281 (-)	251 (-)	−10 (17)	−20 (15)	7 (93)

[a] Anisotropic temperature factors are of the form $\exp[-(\beta_{11}h^2 + \beta_{22}k^2 + \beta_{33}l^2 + 2\beta_{12}hk + 2\beta_{13}hl + 2\beta_{23}kl)]$.

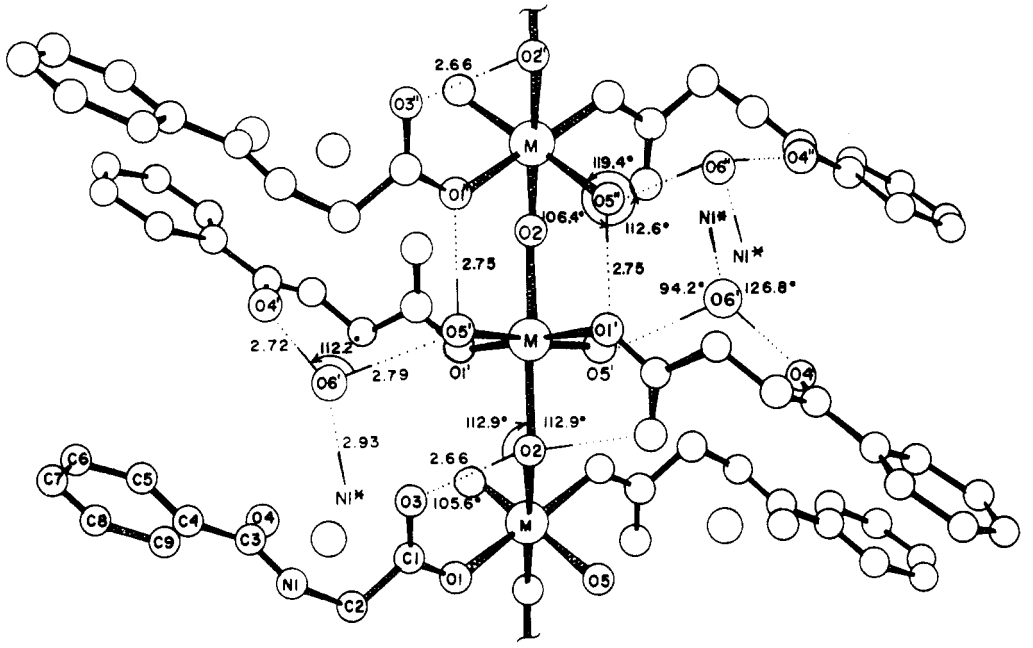

Figure 2. The $Fe(hipp)_2(H_2O)_3 \cdot 2H_2O$ molecule. Hydrogen-bonding interactions are shown as dashed lines, while the solid portion of each dashed line represents the position of the hydrogen atoms.

comparable to those for the nickel analogue. Since the Fe atom occupies a special position in the unit cell, the Fe–Fe separation (4.017 Å) has the same accuracy as that obtained in the unit cell measurements (esd = 0.005 Å).

Figure 1 shows the geometry about the Fe atom. Each iron ion sits on a center of symmetry and is coordinated to six oxygen atoms. Two carboxyl oxygens (Fe–O1 = 2.05 Å) and two nonbridging oxygens (Fe–O5 = 2.11 Å) together with the Fe atom form a plane approximating fourfold symmetry about the iron. These "tetragonal planes" are linked to each other through the oxygen atoms of the bridging water molecules (Fe–O2 = 2.17 Å). The resulting structure is an infinite chain in which alternate tetragonal plates are linked and canted toward each other through Fe–O2–Fe′ bridges. Although canting is equivalent along the b and c axes, the canting angle ϕ (defined as the O2–M–M′ angle for convenience) has a value of 22.5° for the iron hippurate. The longest Fe–O distance is the bridging one (Fe–O2 = 2.17 Å) as would be anticipated.

The backbone of the molecule (···O2–M–O2–M–O2···) extends in an infinite linear chain along the c cell axis. The hippurate molecule is bonded to the iron atom through the carboxyl oxygen atom as has been previously observed in the case of copper hippurate.[10,11] Figure 2 shows the hippurate groups fanning out from the backbone like alternating rungs of a ladder. Since the hippurate ligand is large and bulky, an extensive hydrogen-bonded network was expected to hold the ligand in place. Criteria used in postulating hydrogen bonding are as follows: (1) contact distances should be reasonably short, i.e., less than 3 Å; (2) with the assumption that the hydrogen atoms involved in bonding lie very nearly on the line connecting oxygen atoms, H–O–H angles should be comparable to the normal H–O–H angle of 105°. For example, the lattice water molecule in iron hippurate forms the angle O5–O6–O4 of 112.2° with short contact distances (O5–O6 = 2.79 Å; O4–O6 = 2.72 Å). With use of this type of analysis, both intrachain and interchain hydrogen bonding is postulated to occur (Figure 3 shows the units cell). Intrachain hydrogen bonding involves the following interactions: (1) lattice water molecule (O6–O1, O6–O5) and (2) nonbridging water molecule (two O2–O3). Similarily, interchain hydrogen-bonding interactions are as follows: (1) lattice water molecule (O6–N1*) and (2) nonbridging water molecule (O5–O1*; relatively

(10) J. N. Brown, H. R. Eichelberger, E. Shaeffer, M. L. Good, and L. M. Trefonas, *J. Am. Chem. Soc.*, **93**, 6290 (1971).
(11) J. N. Brown and L. M. Trefonas, *Inorg. Chem.*, **12**, 1730 (1973).

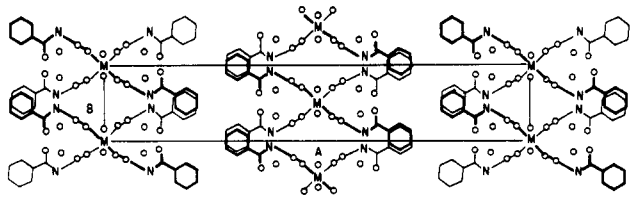

Figure 3. Unit cell of the iron(II), cobalt(II), and nickel(II) hippurates as viewed down the *c* axis. The bold lines are used to illustrate that only two hippurate molecules are bonded to each metal and that they are trans to one another. Although the hippurate configuration is staggered along the *c* axis, all metals in the same *ab* plane have the same hippurate configuration.

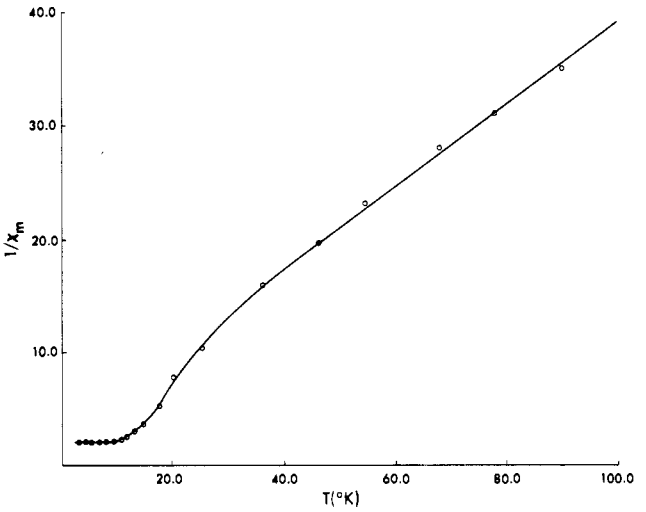

Figure 4. Inverse of the magnetic susceptibility vs. temperature for a powdered sample of $Fe(hipp)_2(H_2O)_3 \cdot 2H_2O$.

weak interaction due to the large distance of 4.5 Å). The lattice water molecule is unique in that it serves not only to anchor the bulky hippurate ligand in place but also to hold chains together along the *b* axis, forming a layer of chains in the *bc* plane. The only interactions between *bc* planes appear to be van der Waals attractions along the *a* axis between the benzene rings of one *bc* plane and the next, resulting in a two-dimensional structure. This type of bonding along the *a* axis is extremely weak (closest interchain benzene–benzene contact distance = 4.2 Å). Consequently, crystallization is retarded along this axis.

Since the Fe, Co, and Ni structures[3] are crystallographically isomorphous, it is of interest to compare their structural similarities and differences. The metal–metal separations of 4.017 Å (Fe–Fe′), 3.996 Å (Co–Co′), and 3.942 Å (Ni–Ni′) parallel the analogous trend in the ionic radii. For all three compounds, the longest M–O distance is the bridging one. However, the values (Fe–O2 = 2.17 Å, Co–O2 = 2.22 Å, and Ni–O2 = 2.12 Å) do not follow the above-mentioned trend in ionic radii. As geometric consequences of the values of this M–O distance, neither the M–O–M′ angles (135.3°, Fe; 128.3°, Co; 137.2°, Ni) nor the canting angles (22.5°, Fe; 25.8°, Co; 21.4°, Ni) follow the trend in ionic radii with the Fe and Ni being most closely related. Another feature that points to the structural similarities of the iron and nickel hippurates arises from the unequal bonding in the previously defined "tetragonal plane". Both the iron hippurate (Fe–O5 = 2.11 Å, Fe–O1 = 2.05 Å; difference = 0.06 Å) and the nickel hippurate (Ni–O5 = 2.07 Å, Ni–O1 = 2.00 Å; difference = 0.07 Å) have the same degree of distortion. In contrast, the cobalt hippurate has fourfold symmetry within experimental error (Co–O5 = 2.06 Å, Co–O1 = 2.04 Å).

Magnetic Properties. The temperature dependence of the magnetic susceptibility is shown in Figure 4. The Curie–Weiss law is obeyed at high temperatures for an $S = 2$ system with a negative Weiss constant ($\mu_{eff} = 4.6\ \mu_B$ and $\Theta = -8.1$ K). At lower temperatures, iron hippurate undergoes a ferromagnetic transition; the magnetic susceptibility appears to saturate just below the temperature of this ferromagnetic transition in external fields as small as 100 Oe. The magnetization isotherms (Figure 5) show field-dependent behavior characteristic of spontaneous magnetization and display a maximum magnetization at 0.9 ± 0.05 emu/g indicating weak ferromagnetism. Since the material saturates easily, data at higher temperatures were used to graphically determine the transition temperature. Constant magnetizations are plotted in Figure 6 and extrapolated to $H_{ext} = 0$ to obtain a transition temperature of 8.1 ± 0.1 K. It is interesting to note that the magnetization isotherms in Figure 5 display field-dependent behavior at temperatures above 8.1 K. A spontaneous magnetic moment can be induced even at room temperature; this net moment was observed to be perpendicular to the chain (*c* axis) by macroscopic observation of the needle crystals in a permanent magnetic field of 5 kOe. A similar observation has also been made for the analogous cobalt(II) and nickel(II) hippurates.

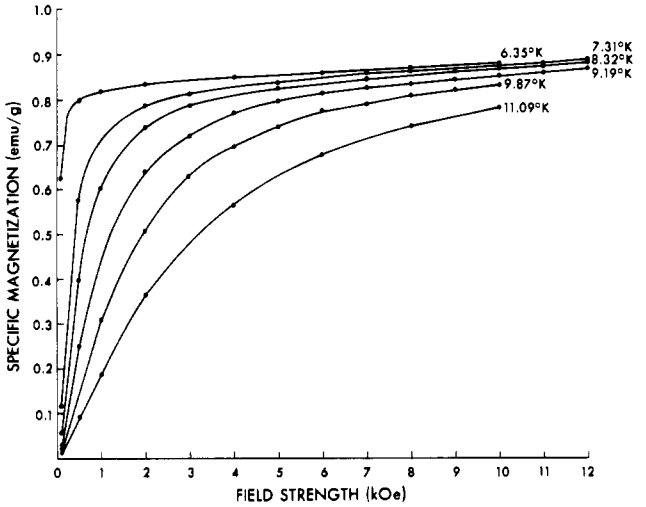

Figure 5. Specific magnetization vs. applied field strength for $Fe(hipp)_2(H_2O)_3 \cdot 2H_2O$ in the region of T_c.

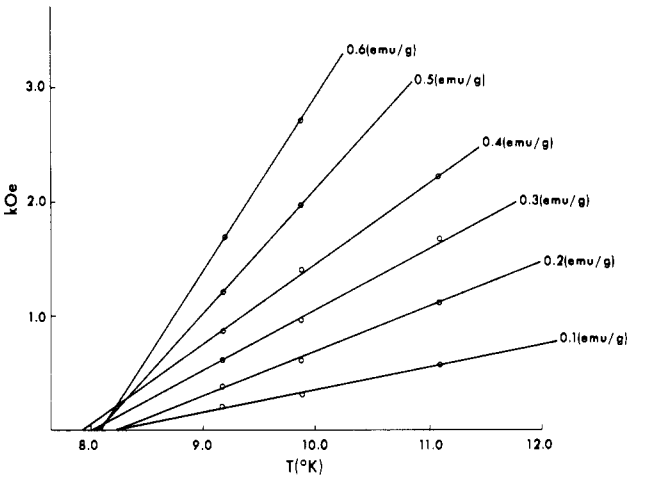

Figure 6. Field strength vs. temperature for $Fe(hipp)_2(H_2O)_3 \cdot 2H_2O$ at constant specific magnetization. Extrapolation to $H = 0$ results in an experimentally determined $T_c = 8.1 \pm 0.05$ K.

Mössbauer Studies. The temperature dependence of the Mössbauer spectrum is shown in Figure 7, and the corresponding parameters are given in Table II. At temperatures much higher than T_c, a nearly symmetrical doublet characteristic of high-spin Fe(II) is observed. This doublet results from a quadrupolar interaction and is composed of two sets

Table II. Mössbauer Data for Iron(II) Hippurate

temp, K	line positions[a]		line widths[a]		quadrupole splitting[a]	isomer shift[a]
	δ_1	δ_2	Γ_1	Γ_2	ΔE	δ
20.01	0.277	2.379	0.346	0.342	2.102	1.328
15.02	0.268	2.384	0.367	0.370	2.116	1.326
4.25	−0.272	2.152	0.425	0.495	2.662[b]	1.331
	0.238	2.697	0.424	0.536		
	0.749		0.369			
1.95	−0.266	2.152	0.416	0.531	2.662[b]	1.329
	0.239	2.694	0.325	0.489		
	0.745		0.346			

[a] All units are in mm/s. [b] Calculated as the difference between the averaged centers of the σ and π transitions.

of transitions (σ and π) involving the nuclear states $|I_z;M_z\rangle$.[12] The $|^1/_2;^1/_2\rangle \rightarrow |^3/_2;^1/_2\rangle$ transitions (quartet) are referred to as the σ set of transitions; the $|^1/_2;^1/_2\rangle \rightarrow |^3/_2;^3/_2\rangle$ doublet is the π set. In the absence of a magnetic field, the degeneracy of these transitions is not lifted, and the usual quadrupole doublet is observed. In a ferromagnetic state, an internal field acts to lift the degeneracy of the σ and π transitions, resulting in a triplet–doublet pattern. Although the iron hippurate system is magnetically ordered below 8.1 K, the type of spectrum displayed in Figure 7 is usually observed when an external field is applied to a rapidly relaxing paramagnet with the condition $H_{int} << \Delta E_Q$ (quadrupole splitting). The apparent triplet is actually the σ quartet, while the higher energy doublet corresponds to the doubly degenerate π transitions. Since the σ transitions occur at lower energy, the sign of the principal component of the electric field gradient (V_{zz}) must be positive. For $H_{int} << \Delta E_Q$, Reiff[12] has shown that the internal magnetic field can be calculated directly from the triplet splitting (Δ_t) by using the relationship

$$H_{int} = 39.29\Delta_t$$

H_{int} was thus determined to be 40.0 kOe at 4.25 and 1.95 K. It should be pointed out that neither ΔE_Q nor Δ_t increases as the temperature is lowered from 4.25 to 1.95 K.

Discussion

Since the nickel, cobalt, and iron hippurates are essentially isostructural, their magnetic behaviors (obviously moderated by single-ion effects) would be expected to be similar in that primary magnetic interactions arise from structural and symmetry considerations. The qualitative model proposed earlier[3] for the nickel and cobalt hippurates consisted of three basic interactions: (1) *intrachain*, isotropic superexchange; (2) *intrachain*, anisotropic superexchange; (3) *interchain*, dipole–dipole exchange. It was proposed that the intrachain interactions could have both isotropic and anisotropic contributions.

Isotropic superexchange causes the normal antiferromagnetic ordering of spins; the interaction is symmetric and expressed as[13]

$$\mathcal{H} = -2J^s\vec{S}_i\vec{S}_j \qquad (1)$$

where J^s is the superexchange spin coupling parameter. Anderson[14] theoretically developed a general set of rules for isotropic superexchange. The theory was based on the orbital overlap involved in the superexchange pathway. For a 180° bridging M–X–M′ angle, J is expected to be large and negative

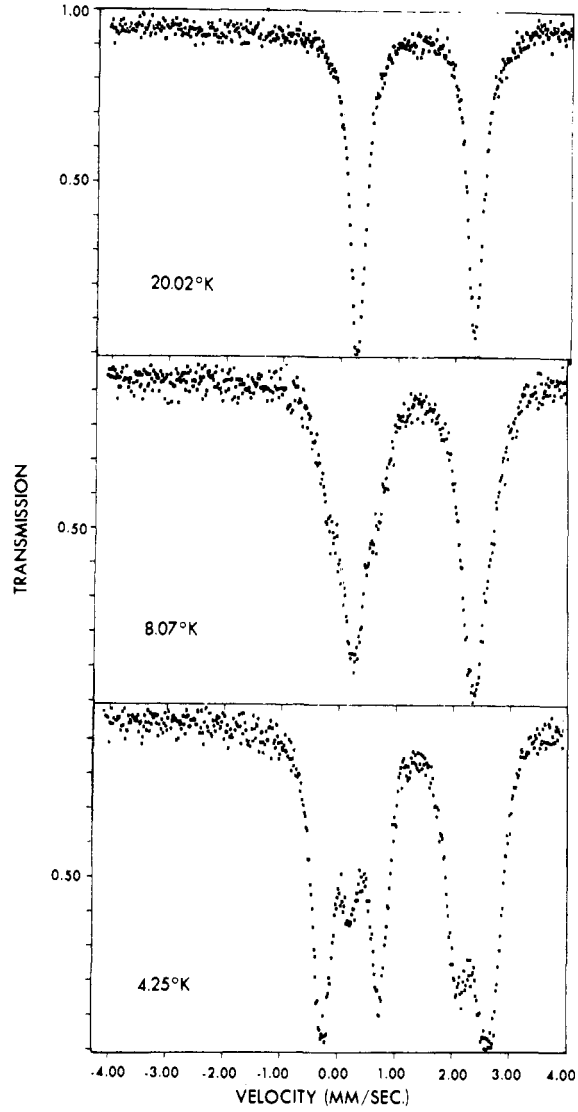

Figure 7. Mössbauer spectra of $Fe(hipp)_2(H_2O)_3 \cdot 2H_2O$: top, 20.01 K; middle, 8.10 K; bottom, 1.95 K.

(antiferromagnetic); conversely, J is predicted to be much smaller and positive (ferromagnetic) for a 90° bridge angle. Anderson's theory has been experimentally confirmed by extensive studies on the Cu(II) and Cr(III) M–X–M′ systems.[15] Antiferromagnetic coupling is at a maximum with a bridging angle of 180° and decreases as the angle decreases; i.e., spin coupling depends upon the nonorthogonality of the orbitals involved in the superexchange pathway. At 97–98° the coupling becomes ferromagnetic with a maximum observed at 90°. Hoffmann and co-workers[14c] have refined the theory of maximum coupling, and although they have confirmed Anderson's predictions qualitatively, the angle leading to maximum ferromagnetic exchange is generally somewhat greater than 90°. However, since the M–O2–M′ angle (θ = 135.3° (Fe), 128.3° (Co), 137.2° (Ni)) is much greater than 100° in all three metal hippurate molecules, isotropic superexchange along the chain (c axis) should be antiferromagnetic with the sign of J^s negative.

The second possible intrachain interaction is anisotropic superexchange. Anisotropic superexchange, commonly referred to as the Dzyaloshinsky–Moriya or D–M interaction,[4,5] arises when the following conditions are met: (1) metal ions cannot be related to one another by a center of symmetry; (2)

(12) W. M. Reiff, *Coord. Chem. Rev.*, **10**, 37 (1973).
(13) R. L. Carlin and A. J. Von Duyneveldt, "Magnetic Properties of Transition Metal Compounds", Springer-Verlag, New York, 1977.
(14) (a) P. W. Anderson, *Magnetism*, **1**, Chapter 2 (1963); (b) P. W. Anderson, *Solid State Phys.*, **14**, 99 (1963); (c) R. H. Summerville and R. Hoffmann, *J. Am. Chem. Soc.*, **101**, 3821 (1979), and references cited therein.
(15) E. A. Boudreaux and L. M. Mulay, Eds., "Theory and Applications of Molecular Paramagnetism", Wiley, New York, 1976, Chapter 7.

there is some single-ion anisotropy ($J^{DM}\alpha g - 2/g$). When these conditions exist, a net moment is spontaneously built up perpendicular to the easy axis of magnetization as a result of AF superexchange ordering. Moriya showed that the mechanism for this phenomenon is primarily antisymmetric spin exchange and could be expressed as[5]

$$\mathcal{H} = J^{DM} \cdot [\vec{S}_i \times \vec{S}_j] \quad (2)$$

This coupling acts to cant the spins away from the normal antiferromagnetic configuration because the coupling energy is minimized when the two spins are perpendicular to each other. Moriya developed the relationship between crystal symmetry and the antisymmetric spin coupling mechanism. With use of this model for the iron, cobalt, and nickel hippurates, the spontaneous moment is predicted to be built up prependicular to the C_2 axis that bisects a line between two neighboring metals and passes through the oxygen atom of the bridging water molecule.

The magnetic susceptibility (Figure 4) exhibits a ferromagnetic transition with the transition temperature being graphically determined to be 8.1 ± 0.1 K. The Curie–Weiss constant is negative (Θ = 8.1 K), which is sometimes interpreted as arising from antiferromagnetic short-range interactions. The superexchange ordering saturates just below the transition temperature in fields as low as 100 Oe; the sharpness of this ordering is indicative of the Ising-like behavior (spin dimensionality = 1) expected for the Fe(II) ion.[16] The magnetization isotherms in Figure 5 show the field-dependent behavior of iron hippurate and are characteristic of a spontaneously magnetized material. In fields of up to 12 kOe, the maximum magnetization attained is only 0.9 emu/g or 0.08 μ_B/Fe atom. A spontaneous moment of 0.08 μ_B is only 2% of the nominal value (4 μ_B for $S = 2$) and corresponds to the weak ferromagnetism associated with the expected D–M interaction (which correlates with the Mössbauer data given below).

For materials in which the D–M interaction is important, Moriya[5] showed that the paramagnetic susceptibility ($T > T_c$) exhibits a very sharp increase in $\chi_\perp$ near T_c. A good example of this phenomenon is $CsCoCl_3 \cdot 2H_2O$; Herweijer and coworkers[17] experimentally observed an induced net spontaneous moment up to temperatures 20° higher than T_c. The observation of the D–M moment above T_c is attributed to the fact that short-range spin correlations associated with the superexchange ordering begin to occur at temperatures much higher than the critical temperature (the temperature below which long-range spin correlations exist). Moriya also showed that the smaller the net spontaneous moment below T_c, the sharper is the increase of $\chi_\perp$ near T_c. Since the spontaneous moment for the hippurate molecule is extremely small below T_c (μ = 0.08 μ_B), a very sharp increase in $\chi_\perp$ is expected above T_c. At room temperature and in the presence of a 5-kOe field, the iron hippurate crystals show a macroscopic alignment perpendicular to the c crystal axis. This behavior would not be expected for a paramagnetic system of this structure. According to Moriya's rules (discussed earlier) and this macroscopic observation, the D–M moment must be directed parallel to the crystallographic a axis.

The Mössbauer spectra (Figure 7) provide additional evidence for the magnetic ordering of spins since changes in the spectra as a function of temperature can be correlated with changes in the magnetic susceptibility. In the paramagnetic region ($T > T_c$), the observed quadrupole doublet is characteristic of high-spin Fe(II). As the temperature is lowered to T_c, the low-energy σ transition broadens. Below T_c, the quadrupole doublet is magnetically split (H_{int} = 40 kOe) into an apparent triplet–doublet pattern consistent with V_{zz} positive.

For V_{zz} positive, Blume[18,19] has shown that in the case of an axially symmetric electric field gradient tensor, initial broadening of the σ transitions (see Results) corresponds to a fluctuating magnetic field oriented perpendicular to the V_{zz} axis. Although this phenomenon can result from slow single-ion paramagnetic relaxation, the relationship between the magnetic susceptibility and Mössbauer data is consistent with the view that the fluctuating magnetic field is due to the one-dimensional superexchange ordering along the chain. A very similar example of superexchange-broadened Mössbauer spectra has been reported for the $Fe(N_2H_5)_2(SO_4)_2$ chain molecule.[20] Consequently, we *assume* that the principal axis of the electric field gradient is perpendicular to the chain or c axis. Therefore, we have assigned the principal axis of the EFG to be coincident with the hipp–Fe–hipp axis for two reasons: (1) the hipp–Fe–hipp axis is the highest axis of symmetry with four water molecules in the x–y plane (approximately D_{4h}); conversely, the nonbridging H_2O–Fe–H_2O axis possesses two different ligands in the x–y plane with the larger differences in bond distances (approximately D_{2h}). (2) In a crystal field approach, V_{zz} positive corresponds to a tetragonal *compression*, which is in agreement with the short Fe–hipp bond distance.

According to crystal field theory, tetragonal compression in D_{4h} serves to split the $^5T_{2g}$ manifold such that the $^5B_{2g}$ term (d_{xy} orbital) lies lower in energy than the ^5E_g (d_{xz}, d_{yz} orbitals) term. Since the tetragonal compression is not large, a considerable amount of spin–orbit coupling is expected to mix the orbitals of the $^5B_{2g}$ and ^2E_g terms. Such mixing reduces the magnitude of V_{zz} and thus ΔE_Q.[12] The small ΔE_Q of 2.1 mm/s at 20 K is indicative of a large amount of spin–orbit coupling. ΔE_Q increases dramatically below T_c to 2.6 mm/s and indicates significant quenching of spin–orbit coupling. Since the increase in ΔE parallels the onset of magnetic ordering, the decrease in spin–orbit coupling appears to be a result of the superexchange phenomenon. It is interesting to note that as the temperature is further lowered, ΔE and Δ_t (the triplet splitting due to the internal magnetic field) remain constant. These observations are consistent with the superexchange saturation observed in the magnetization data and are indicative of the expected Ising behavior for the Fe(II) ion. Finally, it should be pointed out that the isomer shift remains constant above and below T_c, indicating the absence of a *structural* phase transition.

We shall now consider interchain magnetic interactions. As pointed out earlier, interchain magnetic interactions are limited to dipole–dipole interactions. Since dipolar coupling is proportional to r^{-3}, dipole–dipole interactions are not expected along the a axis (closest M–M* distance is greater than 20 Å). Dipolar interactions along the b axis (closest M–M* distance is about 7 Å) can be approximated with use of the expression[13]

$$\mathcal{H} = \frac{\vec{\mu}_i \vec{\mu}_j}{r_{ij}^3} - \frac{3(\vec{\mu}_i \cdot \vec{r}_{ij})(\vec{\mu}_j \cdot \vec{r}_{ij})}{r_{ij}^5} \approx kT_c \quad (3)$$

With use of μ = 0.08 μ_B/Fe atom and the summation over five nearest neighbors on adjacent chains, the interaction is antiferromagnetic and the transition temperature (for interaction along the b axis) was calculated to be 8.8×10^{-5} K. Consequently, antiferromagnetic dipole–dipole interactions along the b axis are not predicted to occur until $T \rightarrow 0$ K.

(16) L. J. le Jongh and A. R. Miedema, *Adv. Phys.*, **23**, 1 (1974), and references cited therein.
(17) A. Herweijer, W. J. M. de Jonge, A. C. Botterman, A. L. M. Bongaarts, and J. A. Cowen, *Phys. Rev. B: Solid State*, **5**, 4618 (1972).
(18) M. Blume, *Phys. Rev. Lett.*, **18**, 305 (1967).
(19) M. Blume and J. A. Tjon, *Phys. Rev.*, **165**, 446 (1968).
(20) C. Cheng, H. Wong, and W. M. Reiff, *Inorg. Chem.*, **16**, 819 (1977).

In summary, the qualitative model is consistent with the following assumptions: (1) Single-ion magnetic moments lie essentially in the x–y plane defined by the coordinate system of the EFG, i.e., $^5B_{2g}$ (d_{xy}) electronic ground state. (2) Isotropic superexchange aligns the spins antiparallel along the chain or c axis. (3) Anisotropic superexchange occurs along the chain and results in a weak net spontaneous (D–M) moment directed parallel to the crystallographic a cell axis (in accordance with Moriya's rules). (4) A sharp saturation in the superexchange ordering below T_c (as seen in the magnetic susceptibility and Mössbauer spectra) indicates the Ising behavior of the Fe(II) ion. (5) Interchain interactions are not predicted to occur until $T \rightarrow 0$ K. From these results we conclude that the iron hippurate molecule represents the first example of a one-dimensional Ising chain system for which magnetic ordering in the second and third dimensions is not predicted to occur until $T \rightarrow 0$ K.

These studies indicate the utility of providing new series of molecular systems whose properties can be used to evaluate existing theoretical models. Furthermore, an understanding of the relationship between structure and magnetic properties can be used in the strategic synthesis of new magnetic systems for practical applications.

Acknowledgment. The authors wish to thank Dr. W. M. Reiff for use of the variable-temperature Mössbauer equipment in his laboratory and for the computer analysis of the collected Mössbauer data. The authors are also grateful to Dr. O. F. Griffith for valuable discussions on dipole–dipole magnetic interactions. Partial funding for this work was provided by NSF Grant No. CHE-76-17434-A03.

Registry No. $Fe(hipp)_2(H_2O)_3 \cdot 2H_2O$, 75180-59-5.

Contribution from the Laboratoire de Spectrochimie des Elêments de Transition, ERA No. 672, Université de Paris-Sud, 91405 Orsay, France, and the Laboratoire de Chimie de Coordination, Associé à l'Université Paul Sabatier, 31030 Toulouse, France

Crystal Structure and Magnetic and EPR Properties of the Heterobinuclear Complex $CuNi(fsa)_2en(H_2O)_2 \cdot H_2O$ ($H_4(fsa)_2en$ = *N,N'*-Bis(2-hydroxy-3-carboxybenzylidene)-1,2-diaminoethane)

I. MORGENSTERN-BADARAU,*[1a] M. RERAT,[1a] O. KAHN,*[1a] J. JAUD,[1b] and J. GALY*[1b]

Received November 3, 1981

The goal of this paper is to investigate the exchange interaction in $CuNi(fsa)_2en(H_2O)_2 \cdot H_2O$, denoted [CuNi], where $(fsa)_2en^{4-}$ is the bichelating ligand derived from the Schiff base *N,N'*-(1-hydroxy-2-carboxybenzylidene)-1,2-diaminoethane. For a comparison of the structure of the pair states in [CuNi] with those of Cu(II) and Ni(II) single-ion ground states, $CuMg(fsa)_2en(H_2O)_2 \cdot H_2O$ and $Ni_2(fsa)_2en(H_2O)_2 \cdot H_2O$, denoted [CuMg] and [NiNi], have also been investigated. The crystal structure of [CuNi] has been solved at −120 °C from 8428 reflections. [CuNi] crystallizes in the trigonal system, space group $P3_1$. The lattice constants are a = 12.8071 (4) Å and c = 9.8157 (8) Å with Z = 3. The structure is made of [CuNi] binuclear units, in which the copper atom is in a strictly planar $-N_2O_2$ environment and the nickel atom in a pseudooctahedral $-O_2O_2(H_2O)_2$ environment. The crystal structure of [NiNi] has been solved at room temperature from 3262 reflections. The space group is $P3_2$, and the structure of the binuclear units [NiNi] is very close to that of the units [CuNi]. The temperature dependence of the magnetic susceptibility of [CuNi], studied in the temperature range 4–300 K, has revealed an energy gap of $-3J/2$ = 213 cm^{-1} between the $^2A_1$ ground state and the $^4A_1$ excited state. The average values of the g factors for the two pair states have been compared to those of the single ions, as deduced from the magnetic behavior of [CuMg] and [NiNi]. The EPR powder spectrum of [CuNi] is typical of an axial symmetry. The single-crystal spectra at 4 K exhibit only one signal for any orientation, assigned to the ground-pair doublet state. The **g** tensor is axial with the unique axis perpendicular to the $N_2CuO_2NiO_2$ pseudo molecular plane. The principal values are $g_\parallel$ = 2.22 (5) and $g_\perp$ = 2.30 (0). The signal broadens out against the temperature in an inhomogeneous manner, the broadening being more pronounced on the high-field side. The magnetic and the EPR data are compared. The *status* of the spin Hamiltonian utilized to interpret these data is discussed. Finally, the mechanism of the exchange interaction is specified. The existence of two exchange pathways, namely, $J_{b_1b_1}$ and $J_{b_1a_1}$, the former being antiferromagnetic and the latter ferromagnetic, is emphasized.

Introduction

If a large interest continues to be taken in the binuclear complexes with identical paramagnetic metallic ions, an evolution started half a decade ago toward the heterobimetallic complexes. Significant theoretical progress concerning the mechanism of the interaction was achieved owing to the study of such compounds;[2,3] much more may be expected.

This field of the heterbinuclear complexes with paramagnetic centers if still limited today by the small number of known and fully structurally characterized compounds and by the relative difficulty of synthesizing new compounds.[4] Probably, it is one of the reasons why some groups focus on doped systems,[5-10] for instance, a few percent of Ni^{2+} in a $[Cu^{II}Cu^{II}]$ matrix or a few percent of Cu^{2+} in a $[Ni^{II}Ni^{II}]$ matrix. The EPR is then a quite appropriate technique to investigate the very low-lying states in the $[Cu^{II}Ni^{II}]$ pairs. Moreover, the magnetic dilution often enables the observation of hyperfine structure, which can itself provide information

(1) (a) Université de Paris-Sud. (b) Université Paul Sabatier.
(2) Kahn, O.; Galy, J.; Journaux, Y.; Jaud, J.; Morgenstern-Badarau, I. *J. Am. Chem. Soc.* **1982**, *104*, 2165.
(3) Journaux, Y.; Coudanne, H.; Kahn, O. *Angew. Chem., Int. Ed. Engl.*, in press.
(4) Casellato, U.; Vigato, P. A.; Fenton, D. E.; Vidali, M. *Chem. Soc. Rev.* **1979**, *8*, 199 and references therein.
(5) Paulson, J. A.; Krost, D. A.; McPherson, G. L.; Rogers, R. D.; Atwood, J. L. *Inorg. Chem.* **1980**, *19*, 2519.
(6) Banci, L.; Bencini, A.; Dei, A.; Gatteschi, D. *Inorg. Chem.* **1981**, *20*, 393.
(7) Buluggiu, E. *J. Phys. Chem. Solids* **1980**, *41*, 43, 1175.
(8) Banci, L.; Bencini, A.; Benelli, C.; Dei, A.; Gatteschi, D. *Inorg. Chem.* **1981**, *20*, 1399.
(9) Kokoszka, G. E.; Allen, H. C., Jr.; Gordon, G. *J. Chem. Phys.* **1967**, *46*, 3020.
(10) Banci, L.; Bencini, A.; Gatteschi, D. *Inorg. Chem.* **1981**, *20*, 2734.

0020-1669/82/1321-3050$01.25/0 © 1982 American Chemical Society